Investigation and Visualization of Internal Flow through Particle Aggregates and Microbial Flocs using Particle Image Velocimetry

Feng Xiao[a,b], Kit Ming Lam[a], Xiao-yan Li[a,*]

[a]Environmental Engineering Research Centre, Department of Civil Engineering,

The University of Hong Kong, Pokfulam Road, Hong Kong, China

[b]State Key Laboratory of Environmental Aquatic Chemistry, Research Center for Eco-Environmental

Sciences, Chinese Academy of Sciences, 18 Shuangqing Road, Beijing 100085, China

(*Corresponding author: phone: 852-28592659; fax: 852-28595337; e-mail: xlia@hkucc.hku.hk)

ABSTRACT: An advanced particle-tracking and flow-visualization technology, particle image velocimetry (PIV), was utilized to investigate the hydrodynamic properties of large aggregates in water. The laser-based PIV system was used together with a settling column to capture the streamlines around two types of aggregates: latex particle aggregates and activated sludge (AS) flocs. Both types of the aggregates were highly porous and fractal with fractal dimensions of 2.13 $\pm$ 0.31 for the latex particle aggregates (1210 - 2144 μm) and 1.78 $\pm$ 0.24 for the AS flocs (1265 - 3737 μm). The results show that PIV is a powerful flow visualization technique capable of determining flow field details at the micrometer scale around and through settling aggregates and flocs. The PIV streamlines provided direct experimental proof of internal flow through the aggregate interiors. According to the PIV images, fluid collection efficiency ranged from 0.052 to 0.174 for the latex particle aggregates and from 0.008 to 0.126 for AS flocs. AS flocs are apparently less permeable than the particle aggregates, probably due to the extracellular polymeric substances (EPS) produced by bacteria clogging the pores within the flocs. The internal permeation of fractal aggregates and bio-flocs would enhance flocculation between particles and material transport into the aggregates.

KEYWORDS: Activated sludge; aggregates; fluid collection efficiency; fractal dimension; particle image velocimetry (PIV); permeability; streamlines.

1. Introduction

Aggregates, or flocs, composed of small particles and/or microbial cells, play an important role in the sedimentation of particulate matter in natural waters and in solids-liquid separation in water and wastewater treatment systems. Research has shown that particle aggregates are porous with a fractal structure [1-4]. Given their great porosity, large aggregates would allow fluid to flow through their interiors, which would give rise to different hydrodynamic behavior compared to that of otherwise solid spheres. This internal permeation of large aggregates can enhance the particle flocculation and mass transfer processes. Thus, knowledge about the permeability of large aggregates is essential to the description of aggregate hydrodynamics and the modeling of the coagulation kinetics in a particle system [5-7].

Theoretical work on characterizing the permeability of particles began with Brinkman's analytical study [8]. Adler estimated internal flow through porous spheres based on Darcy's law and Brinkman's equation [9]. Neale et al. proposed a cell model to analyze the movement of a permeable floc as a swarm of moving particles [10], while Veerapaneni and Wiesner developed a multilayer model that divided a floc into several shells, each with a different porosity and permeability [11]. Li and Logan employed a fractal scaling concept and proposed a cluster-cluster structure to model aggregate permeability [12]. Recently, the computational fluid dynamic method has been used to determine internal flow through particle aggregates [13-15]. However, most of these model predications have not been experimentally validated.

Settling velocity measurement has been used as a technique to determine the permeability of particle aggregates and microbial flocs [16, 17]. Li and Yuan used a double settling column with fluids of different densities to characterize the settling behavior of activated sludge flocs [18].

Their results showed that the settling velocity of the bio-flocs was only slightly faster than predicted by Stokes' law for impermeable spheres of the same size and density. Zhang et al. [19] and Xiao et al. [20] also reported low permeability values for anaerobic and aerobic granules based on the settling velocity measurement. However, the settling experiment method relies on the assumption of a certain aggregate structure and some permeability models that have not been verified. In addition, determining the density of an aggregate in water is rather difficult, which affects the calculation accuracy of Stokes' settling velocity for the aggregates.

Efforts have been made to directly visualize internal flow through individual aggregates. A bubble-tracking technique has been used to illustrate the flow field around settling flocs [21-24]. The rising paths of air bubbles in relation to a falling floc were used to outline the streamlines around the floc. However, air bubbles are too large in size and too light in density to be used as flow tracers. Hence, the bubble-tracking method could not provide accurate streamline details for the flow field around moving aggregates.

Particle image velocimetry (PIV) is a more advanced flow visualization technology [25, 26]. It is a non-intrusive, whole-flow-field technique that provides instantaneous velocity vector measurements on so-called tracer particles suspended in the fluid [27]. Xiao et al. attempted to use PIV to observe the interactions between particles and aggregates in water [28]. More recently, the PIV system has been employed to measure particle size distributions during the dynamic flocculation process [29, 30]. He et al. applied a similar technique to characterize the size evolution of particle flocs in a low-shear flow [31]. The PIV technique is by far the most advanced method capable of capturing the flow field details of particle aggregates. In this experimental study, the PIV-based particle tracking technique was employed to investigate the
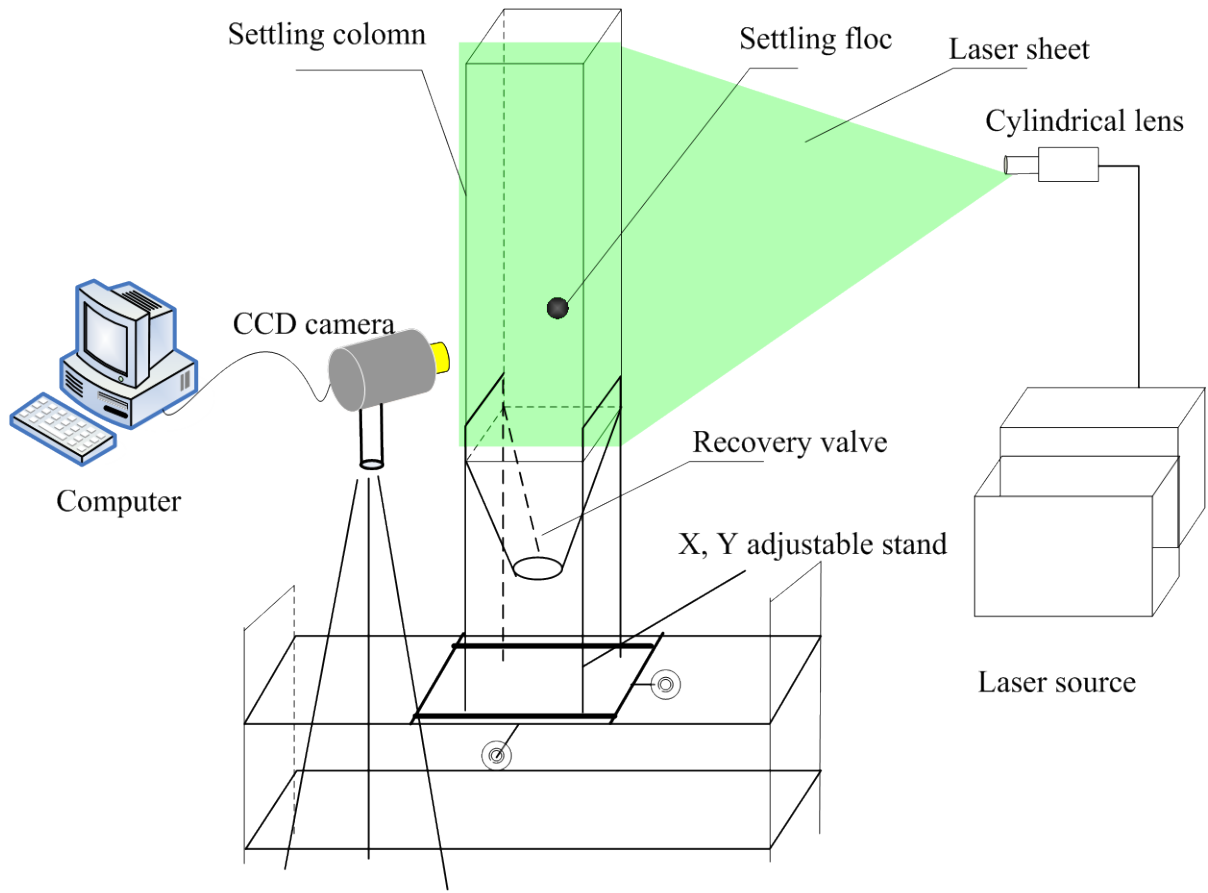
hydrodynamic behavior and permeability of large settling aggregates. Two types of aggregates, latex particle aggregates and activated sludge flocs, were selected for this PIV-settling study.

2. Materials and Methods

2.1 Particle image velocimetry (PIV) system

The PIV system consists of a laser illumination setup (Coherent, Santa Clara, CA), a high-speed CCD video camera (PCO. imaging 1200) and a process control and image processing software package (PCO. camware) (Fig. 1). During the PIV process, "seeding" particles, or tracers, are well suspended in water and particle displacements are detected within a given area of the flow field illuminated by a light sheet. In modern PIV, the illuminating sheet is usually generated using a laser light source equipped with dedicated optic components. The positions of the illuminated tracer particles in motion with the flow are captured by a high-speed CCD camera facing the light sheet. Particles appear as light specks on a dark background in each image frame. Accordingly, the flow field can be tracked and outlined based on the trajectories of the moving tracer particles.

The PIV imaging system was calibrated before the aggregate settling experiments. The calibration involved placing a planar plate with a scaled line grid at the position of the laser illumination sheet in the water column to facilitate photography. Based on the grid scales, the PIV images were sized accurately. The full PIV view had dimensions of 11.2×9.8 mm^2. Because the images were composed of 1280×1024 pixels, the resolution of each pixel was about 8.8×9.6 µm^2, which was about the size of the tracer particles.
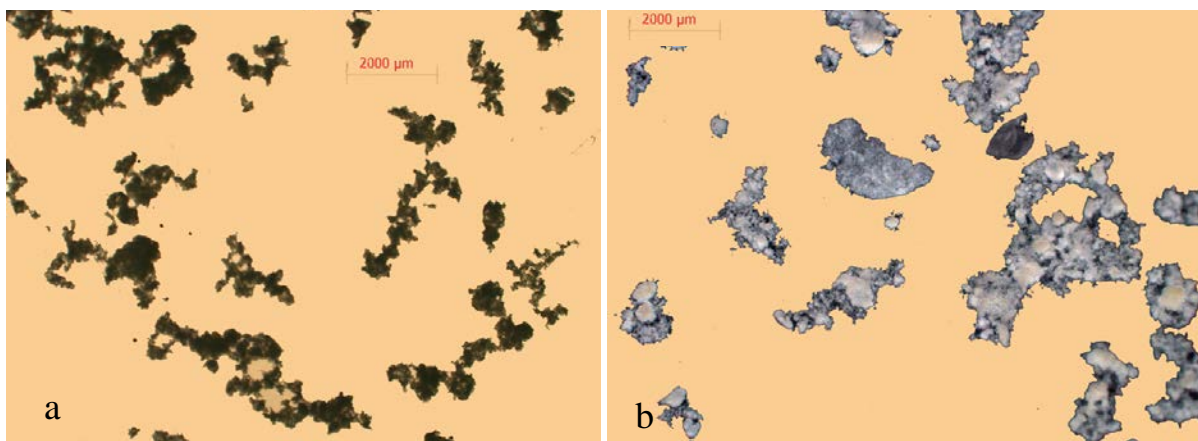
Fig. 1. Schematics of the PIV setup for experiments in the settling column.

2.2 Generation of particle aggregates and microbial flocs

A standard jar-test device (ZR4-6, Zhongrun Co., Shenzhen, China) was used for flocculation to produce large aggregates. The jar-tester consisted of six 1 L beakers for which water stirring was provided by flat paddle mixers (5.0 × 4.0 cm^2) rotating at 20 rpm. Two types of large aggregates, latex particle aggregates and activated sludge (AS) flocs, were produced for these settling experiments. For particle aggregation, standard latex microspheres with a diameter of 2.87 μm and a density of 1.05 g/cm^3 (Polysciences) were added to 500 mL tap water at a mass concentration of around 30 mg/L. A low dose of ferric iron (FeCl$_3$) (UNI-Chem) was added at a

concentration of 1 mg/L as the flocculent [32]. Large particle aggregates formed after 15 min of the jar-test flocculation (Fig. 2a). For the AS flocs, raw activated sludge was collected from a local municipal wastewater treatment plant (Stanley Sewage Treatment Works, Hong Kong). The sludge was diluted in tap water to around 100 mg/L and further flocculated using the jar-tester to form larger AS flocs (Fig. 2b) for the settling experiments.

Fig. 2. Microscopic images of (a) aggregates of latex microspheres and (b) flocs of activated sludge.

2.3 PIV-settling experiments

The PIV-settling experiments were conducted in the settling column, which was filled with water having a density of 0.997 g/cm^3 at 22 ^{o}C. During the settling experiment, an aggregate, either a latex particle aggregate or an AS floc, was placed gently, using a dropper, at the top of the settling column. The column was placed on a stand that could be adjusted gently to ensure the vertical PIV laser illumination sheet through the center of the falling aggregate in the column. The aggregates and flocs were able to reach their terminal falling velocity within 5 cm from the
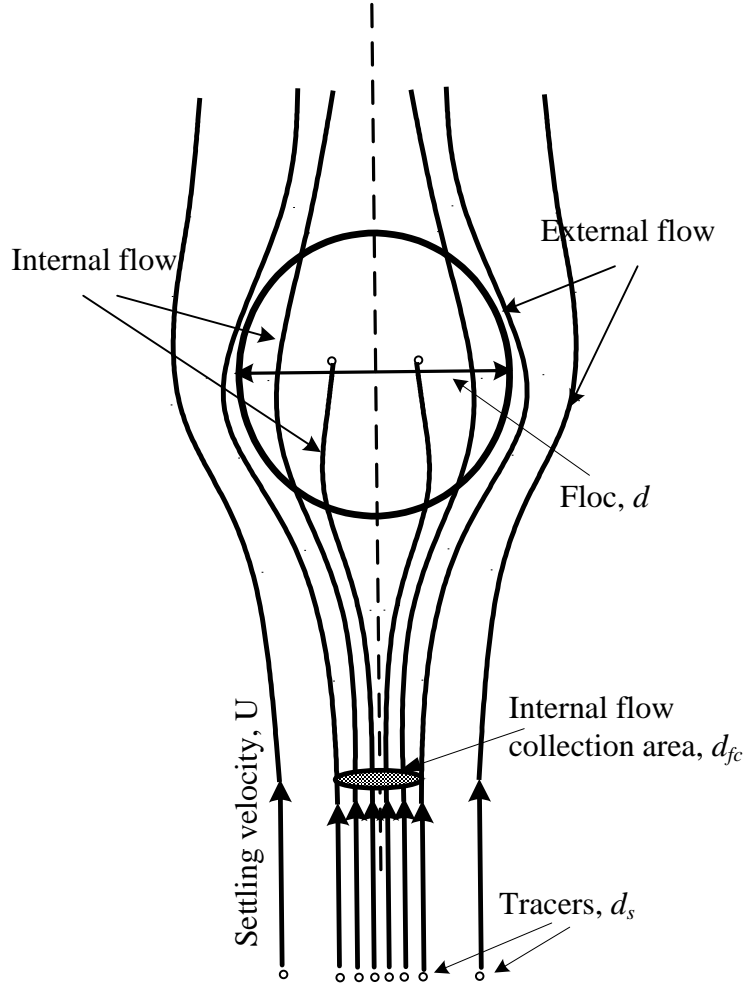
top of the column. When an aggregate fell through the CCD camera's view field, the settling of the aggregate and the movements of the tracer particles brought about by the aggregate settling were recorded (video clip samples - Supplementary Material). Tracking the flow tracers from the PIV images allowed the determination of streamlines around and through the falling aggregate.

The PIV image of each particle aggregate or AS floc was analyzed for size. For an aggregate of irregular shape, the enclosed area in the projected PIV image, A, was determined using an image processing system (PCO. camware). The size of the aggregate was then defined as the area-based equivalent diameter, e.g., $d = \sqrt{4A/\pi}$. Moreover, the terminal settling velocity, U, of the aggregate was calculated from the PIV video recording of it settling in the water column.

2.4 Determination of the streamlines and internal flow

The PIV images were analyzed to outline the detail movements of flow tracers induced by falling aggregates. As a way of analysis, a fixed coordinator was set up at the center of the falling object. The positions of relevant tracer particles were then digitized using WINDIG software, developed by Lovy from the University of Geneva (http://www.unige.ch/sciences/chifi/cpb/windig.html), which is by far one of the most effective software tools for extracting data from graphs. The abovementioned procedure was then repeated on consecutive PIV images. The positions of the trace particles in different images displayed the apparent displacement caused by the falling aggregate. Accordingly, the digitized points for the same tracer particles were connected, which formed trajectory curves for the flow tracers relative to the falling object. A group of these trajectory curves illustrate the flow field, i.e., streamlines, around the falling aggregate (Fig. 3).

Fig. 3. Illustration of the streamlines around and through a permeable aggregate and determination of the fluid collection efficiency of falling aggregates.

The internal permeation of a permeable aggregate can be specified using fluid collection efficiency (η), which is the ratio of the flow passing through the aggregate to the flow approaching it [11]. Fluid collection efficiency can be estimated from the streamlines around and through the aggregate, or $\eta = (d_{fc}/d)^2$, where d_{fc} is the span of the streamlines flowing into the aggregate relative to the span of the streamlines (d) approaching it (Fig. 3). With the PIV technique, the internal flow through a falling aggregate can be visualized using the streamlines

9

and hence, the fluid collection efficiency of the settling aggregate can be estimated. Apparently, η = 0 means that the aggregate is impermeable, with no streamlines through it, and $\eta > 0$ implies that the aggregate is permeable, with streamlines through its interior.

2.5 Settling velocity and fluid collection efficiency

The aggregates that fell to the bottom of the column were carefully recovered and transferred to a pre-weighted polycarbonate membrane (0.2 μm, Osmonics). Each membrane and aggregate was then dried at 105˚C for 1.5 h and its dry mass, W_d, was measured using an electronic microbalance (AEM-5200, Shimadzu, Japan). For a group of aggregates, the dry mass (W_d) can be related to the size (d) of the aggregates with a fractal dimension, D_f, in

$$W_d = ad^{D_f},$$ (1)

where a is a constant [19, 20, 33]. Then, the fractal dimension D_f can be determined from a log-log plot of dry weight versus aggregate size.

The terminal settling velocity U_s of an impermeable aggregate can be predicted using the following generalization of Stokes' law for a wide range of Reynolds numbers,

$$U_s = \left(\frac{4g(\rho_a - \rho_l)d}{3\rho_l C_d} \right)^{1/2},$$ (2)

where ρ_a and ρ_l are the densities of the aggregate and the liquid, respectively, and g is the gravitational constant [2, 16, 18]. The drag coefficient C_d is adjusted for higher Reynolds numbers ($Re > 1$), according to $C_d = 24/Re + 6/(1 + \sqrt{Re}) + 0.4$ [2]. Regarding the latex particle aggregates, it can be derived that

$$U_s = \left(\frac{8g}{\pi} \left(\frac{1}{\rho_l} - \frac{1}{\rho_p} \right) \frac{W_d}{C_d d^2} \right)^{1/2} , \tag{3}$$

where ρ_p is the density of the latex microspheres forming the aggregates ($\rho_c = 1.05$ g/cm^3).
Regarding AS flocs, it has been determined that

$$U_s = \left(\frac{8gf}{\pi} \left(\frac{1}{\rho_l} - \frac{1}{\rho_c} \right) \frac{W_d}{C_d d^2} \right)^{1/2} , \tag{4}$$

where ρ_c is the density of the (wet) bacterial cells and f is a ratio factor between the wet mass and the dry mass of the cells [18-20]. Values of $f = 3.45$ and $\rho_c = 1.06$ g/cm^3 have been used for aerobic bacteria [18, 20, 33].

Flow through an aggregate can reduce its drag, which results in a settling velocity that is faster than that of an otherwise identical but impermeable object predicted using Stokes' law [34]. The settling velocity of a permeable aggregate, U, can be related to that predicted by Stokes' law, U_s, by

$$\frac{U}{U_s} = \frac{\xi}{\xi - \tanh(\xi)} + \frac{3}{2\xi^2} , \tag{5}$$

where ξ is a dimensionless permeability factor that is a function of the size and permeability (κ) of the aggregate according to $\xi^{-2} = 4\kappa / d^2$ [2]. Subsequently, using the ξ value determined from the settling test, the fluid collection efficiency of the settling aggregate, η, can be calculated by [9, 12, 20]
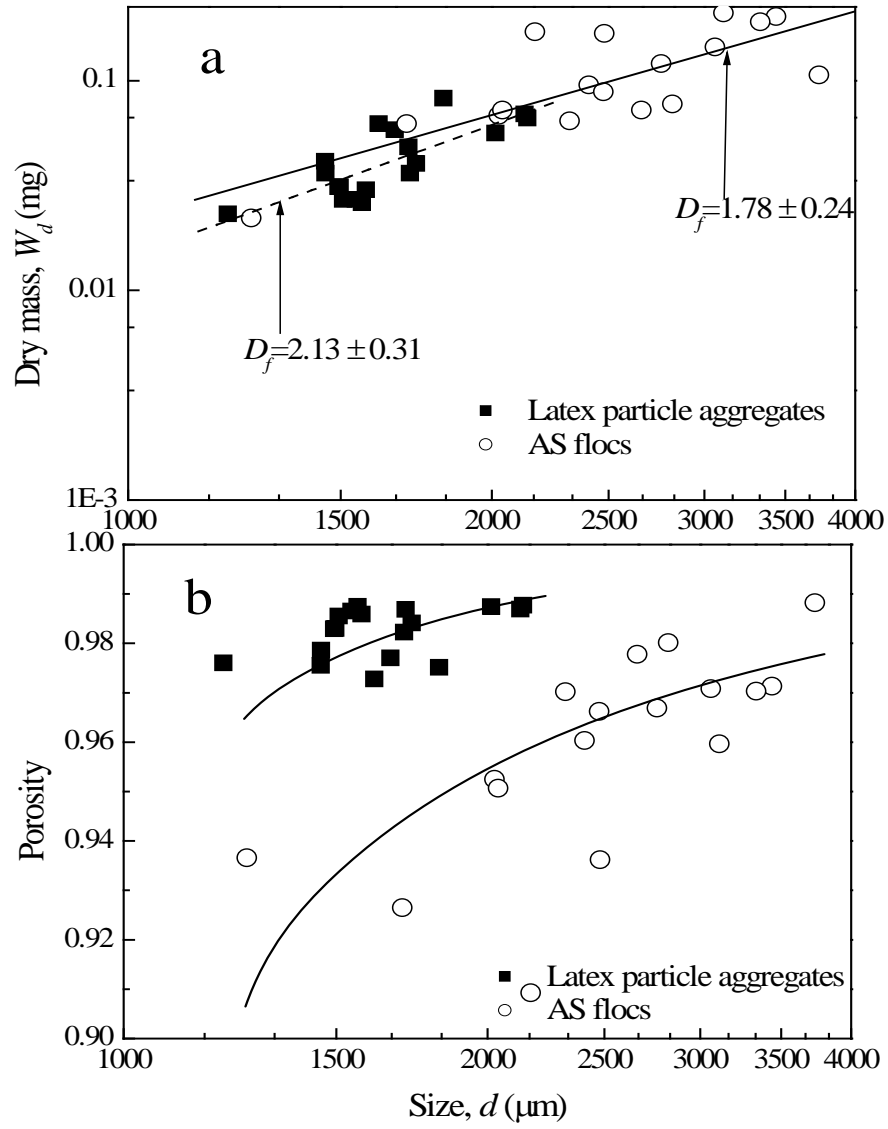
$$\eta = \frac{9(\xi - \tanh(\xi))}{2\xi^3 + 3(\xi - \tanh(\xi))} . \tag{6}$$

11

3. Results and Discussion

3.1 Fractal structure of the aggregates

The porous and fractal structures were identified for the particle aggregates and AS flocs for their irregular shapes and internal pores (Fig. 3). Around 20 typical latex particle aggregates and 20 AS flocs were recovered after the settling experiments and analyzed for their structural properties. The particle aggregates varied in size from 1210.5 to 2144.0 μm and the AS flocs ranged from 1265.9 to 3737.3 μm. Both aggregate types became more porous as they increased in size, with porosities ranging from 0.973 to 0.988 for the latex particle aggregates and from 0.909 to 0.980 for the AS flocs (Fig. 4).

Based on the slope of the logarithmic relationship between the mass and size, the fractal dimensions determined were 2.13 for the latex particle aggregates and 1.78 for the AS flocs (Fig. 4). Generally speaking, a wide range of fractal dimensions, from 1.4 to 2.8, has been reported for particle aggregates and microbial flocs [18, 19, 35-37]. A lower fractal dimension value indicates a looser and more porous aggregate structure and thus a higher interior flow permeation, whereas a higher fractal dimension value suggests a denser and stronger structure.
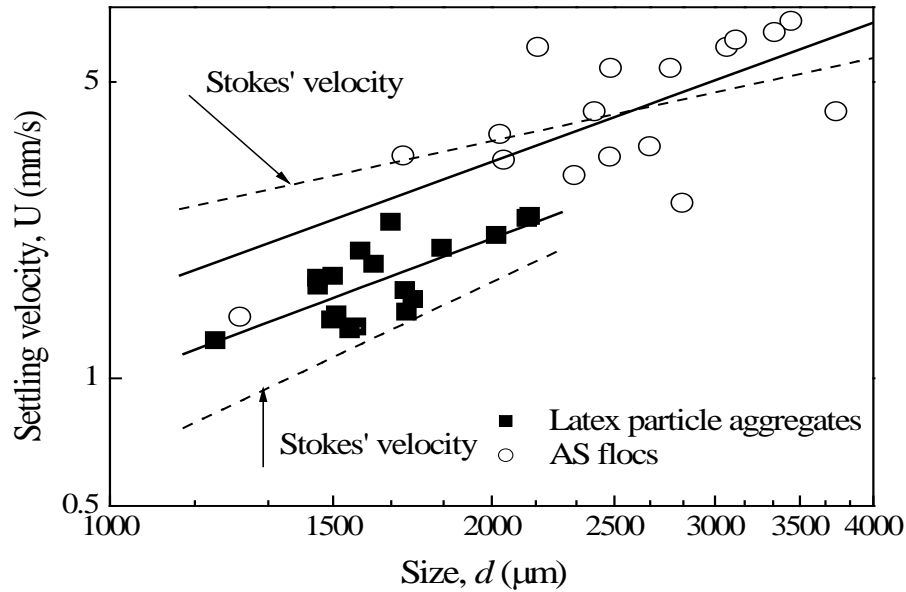
Fig. 4. (a) Dry mass and (b) porosity of the latex particle aggregates and AS flocs as a function of their sizes.

3.2 Settling velocities

The settling velocities of the latex particle aggregates in water varied from 1.23 to 2.41 mm/s and the settling velocities of the AS flocs varied from 1.88 to 6.97 mm/s (Fig. 5). The corresponding Reynolds numbers were within a range of 2.0 - 24.2. The AS flocs settled slightly

faster than the particle aggregates of similar sizes. The slopes of the settling velocity versus size after log-log transformation were 1.12 ($r^2 = 0.73$) for the particle aggregates and 1.09 ($r^2 = 0.71$) for the AS flocs. The settling velocities of the AS flocs agreed better with the predictions of Stokes' law for porous but impermeable particles. The ratios between measured and predicated settling velocities varied from 0.86 to 1.24 with an average of 0.99 ± 0.04. This value close to unity suggests that the internal permeation of the AS flocs might not be significant enough to affect their settling behavior. For the particle aggregates, however, the settling velocities observed were faster than those predicated by Stokes' law for impermeable particles of identical size and mass. The ratios between the measured and Stokes' settling velocities for the particle aggregates ranged from 1.17 to 1.58 with an average of 1.35 ± 0.10. These higher ratios indicate that the particle aggregates endured a lower drag than that expected for impermeable spheres.
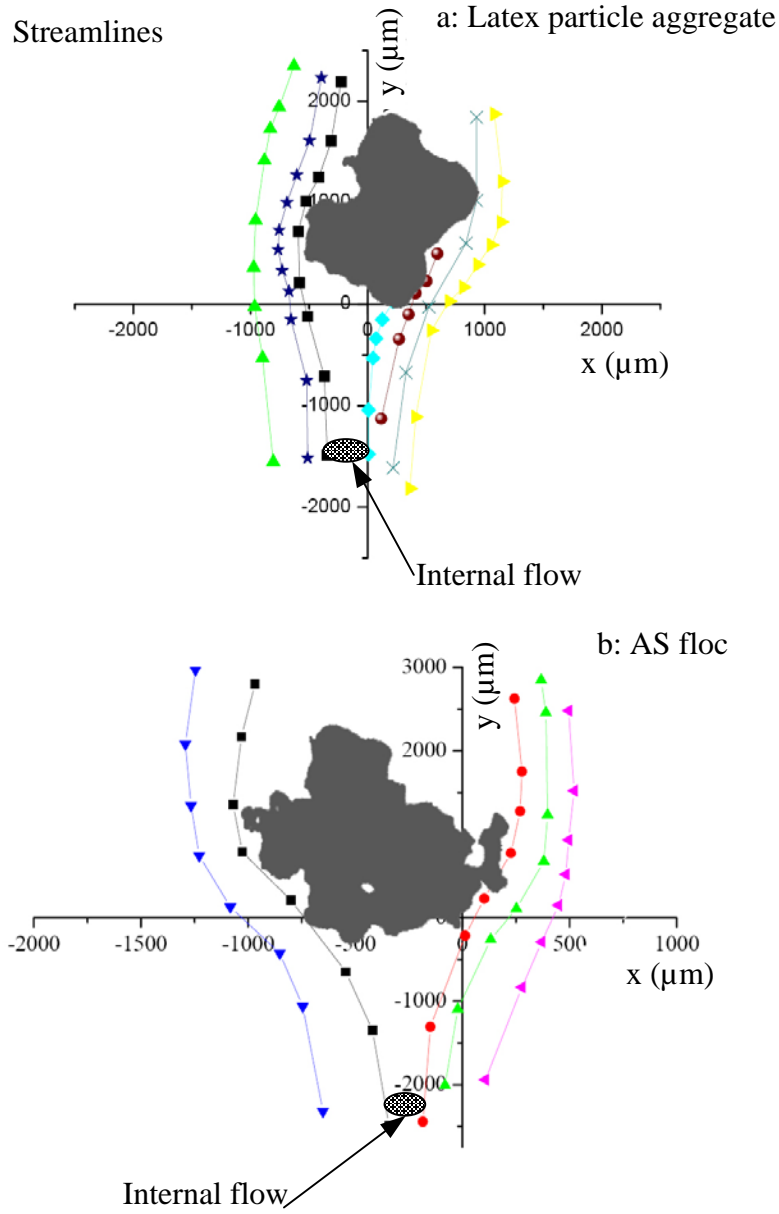

Fig. 5. Settling velocities of the particle aggregates and AS flocs compared to Stokes' law predictions.

The settling velocities of the AS flocs were around 1.5 times faster than those of the latex particle aggregates and the settling test results were generally consistent with values reported in previous studies. Li and Logan observed that the settling velocities of latex particle aggregates ranged from 0.02 to 0.18 cm/s for a size varying from 200 to 1000 μm [16]. Li and Ganczarczyk reported a velocity from 0.03 to 0.20 cm/s for AS flocs with a size ranging from 60 to 1000 μm [38]. Lee et al. measured a settling velocity from 0.02 to 2.0 cm/s for AS flocs with sizes from 0.03 to 12 mm and reported that the settling velocity was proportional to the size of the AS flocs to a power of between 0.7 and 0.8 [35]. Li and Yuan reported settling velocities from 0.22 to 0.64 cm/s for microbial flocs 1.1 to 2.1 mm in diameter and found that the power-law value was 0.94, which is closer to the present value of 1.09 for AS flocs [18].

3.3 Streamlines, internal flow and fluid collection

The streamlines relative to a settling aggregate or AS floc were obtained using the velocity vectors of the seeding tracer particles determined from the PIV images (Fig. 6). The streamlines appeared to be separated into two groups. There were the outside open-flow streamlines, which showed the tracer particles passing around the falling aggregate, and the internal flow streamlines, which showed the tracers moving into the aggregate. Between these external and internal flow streamlines were critical streamlines that showed the tracers sweeping just over the surface of the aggregate. The internal flow through the aggregate interior and the corresponding fluid collection efficiency were determined from the flow fields outlined by these streamlines. For example, Figure 6 shows streamlines obtained for a typical latex particle aggregate (d = 1708 μm) and a typical AS floc (d = 1933 μm).

Streamlines

a: Latex particle aggregate

y (µm)

x (µm)

Internal flow

b: AS floc
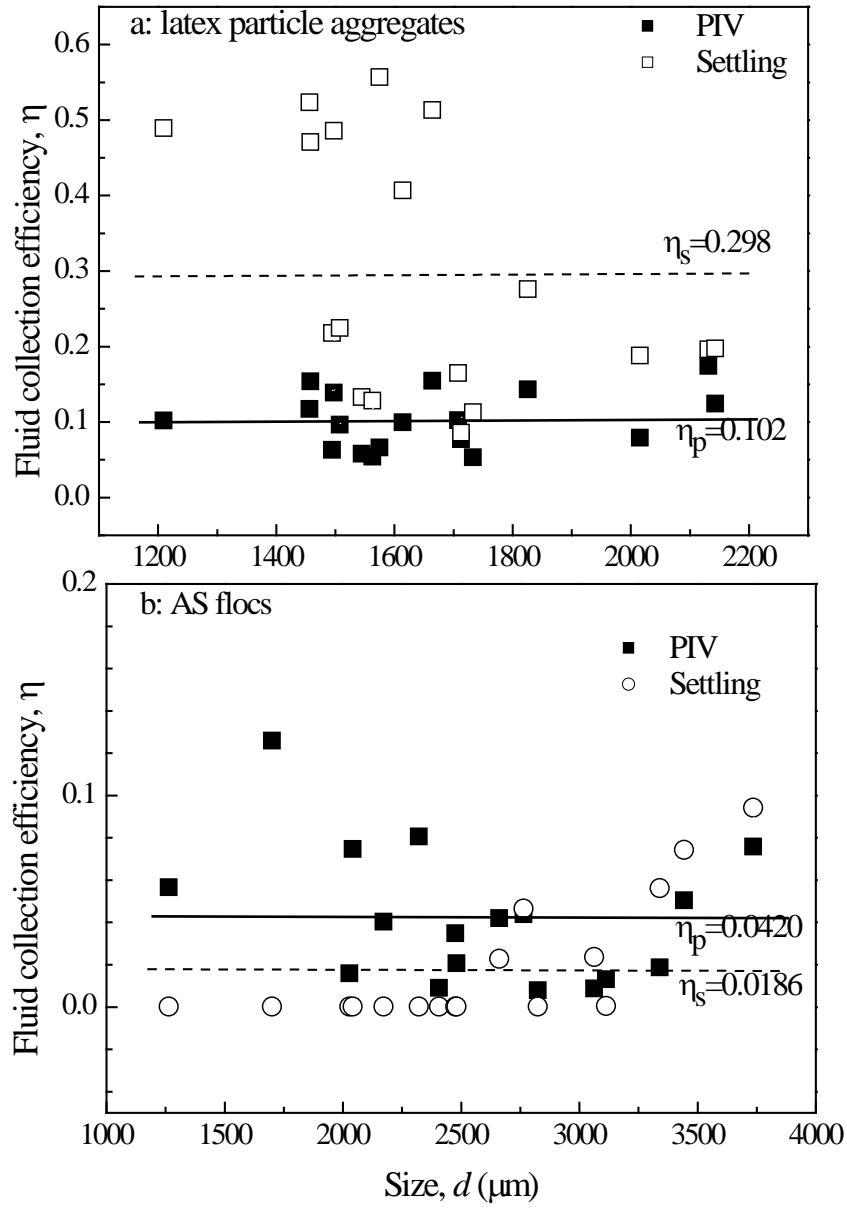
y (µm)

x (µm)

Internal flow

Fig. 6. Determination from PIV images of typical streamlines around (a) a particle aggregate and (b) an AS floc falling in the settling column.

The PIV results provided direct evidence of internal flow through large fractal aggregates. Based on the streamlines, the fluid collection efficiency varied from 0.052 to 0.174 for the latex particle aggregates with an average of $\eta_p = 0.102 \pm 0.020$. The fluid collection efficiency for the

AS flocs ranged from 0.008 to 0.126 with an average of $\eta_p = 0.042 \pm 0.010$ (Fig. 7). The particle aggregates appeared to be more permeable than the AS flocs, which is consistent with previous experimental findings based on the settling velocity measurements. Li and Logan reported a fluid collection efficiency ranging from 0.08 to 0.83 for latex particle aggregates [16], while in the work of Li and Yuan the average fluid collection efficiency was 0.05 for microbial flocs [18]. It has been recognized that the extracellular polymeric substances (EPS) produced by bacteria will form a gel-matrix within bio-flocs, which clogs the interior pores of AS flocs and decreases their permeability [18, 39].

Conventionally, as described in Eqs. 2-6, the fluid collection efficiency of a falling aggregate can be determined using the comparison between its measured settling velocity and predicted Stokes' velocity. The fluid collection efficiencies estimated from the settling velocity comparison ranged from 0.085 to 0.556 for the latex particle aggregates with an average of $\eta_s = 0.298 \pm 0.035$, and from 0 to 0.094 for the AS flocs with an average of $\eta_s = 0.019 \pm 0.004$. There is a certain extent of discrepancy between the PIV method and the settling velocity-based estimation in the determination of fluid collection efficiencies for falling aggregates and flocs (Fig. 7). The difference between these two methods is much more significant for the particle aggregates than for the AS flocs.

Fig. 7. Fluid collection efficiencies of latex particle aggregates and AS flocs determined from PIV streamlines in comparison to those estimated from the settling velocity measurement.

The fluid collection efficiencies determined from the PIV streamlines were about 1/3 lower than those calculated based on the settling velocity measurement of the particle aggregates. It should be noted that the determination of streamlines for some settling aggregates was rather

difficult, and there was a certain degree of error involved in determining internal flow. However, compared to the settling velocity-based estimation, the fluid collection efficiencies determined from the direct PIV observations should prove more reliable and realistic. In addition, while the settling velocity measurement for an aggregate was accurate, its Stokes' velocity could be miscalculated. During the recovery of an aggregate from the bottom of the settling column, the fragile aggregate was easily broken and some portions or pieces of the broken aggregate were not recovered and included in the weight measurement. This underestimation of the dry mass of the latex particle aggregates could result in an underestimation of their Stokes' settling velocities (Eq. 2), which could lead to an overestimation of their internal flow collections. Compared to the particle aggregates, the AS flocs were larger and stronger and their recovery was more reliable and comprehensive. Hence, the fluid collection efficiency values determined by the PIV method and estimated from the settling velocity measurements were more comparable for the AS flocs.

4. Conclusions

- A PIV-based particle-tracking technique was utilized as a powerful flow visualization method to determine streamlines and flow details at the micrometer scale around moving aggregates in water. The PIV streamlines provided direct experimental proof of internal flow through the interiors of large particle aggregates and microbial flocs.

- According to the analysis of PIV images, the average fluid collection efficiency was 0.102 for the latex particle aggregates and 0.042 for AS flocs. The permeable nature of large aggregates and bio-flocs can significantly enhance flocculation between particles and mass transport into the aggregates and bio-flocs.

Acknowledgements

References

[1]   P. Meakin, Adv. Colloid Interface Sci. 28 (1984) 249.

[2]   C.P. Johnson, X.Y. Li, B.E. Logan, Environ. Sci. Technol. 30 (1996) 1911.

[3]   G.C. Bushell, Y.D. Yan, D. Woodfield, J. Raper, R. Amal, Adv. Colloid Interface Sci. 95 (2002) 1.

[4]   W.R. Heinson, C.M. Sorenson, A. Chakrabarti, J. Colloid Interface Sci. 375 (2012) 65.

[5]   M. Vanni, Chem. Eng. Sci. 55 (2000) 685.

[6]   L. Gmachowski, Colloids Surf. A-Physicochemical and Eng. Aspects 225 (2005) 105.

[7]   M.L. Weber-Shirk, L.W. Lion, Water Res. 44 (2010) 5180.

[8]   H.C. Brinkman, Appl. Sci. Res. A-Mechan. Heat Chem. Eng. Math. Methods 1 (1947) 27.

[9]   P.M. Adler, J. Colloid Interface Sci. 83 (1981) 106.

[10]   G. Neal, N. Epstein, W. Nader, Chem. Eng. Sci. 28 (1973) 1865.

[11]   S.Veerapaneni, M.R. Wiesner, J. Colloid Interface Sci. 177 (1996) 45.

[12]   X.Y. Li, B.E. Logan, Water Res. 35 (2001) 3373.

[13]   R.M. Wu, D.J. Lee, Chem. Eng. Sci. 53 (1998) 3571.

[14]   J.P. Hsu, Y.H. Hsieh, J. Colloid Interface Sci. 259 (2003) 301.

[15] L. Liu, G.P. Sheng, W.W. Li, J. Zeng, H.Q. Yu, AIChE J. 57 (2011) 2909.

[16] X.Y. Li, B.E. Logan, Environ. Sci. Technol. 31 (1997) 1229.

[17] M. Hribersek, B. Zajdela, A. Hribernik, M. Zadravec, Water Res. 45 (2011) 1729.

[18] X.Y. Li, Y. Yuan, Environ. Sci. Technol. 36 (2002) 387.

[19] J.J. Zhang, X.Y. Li, S.E. Oh, B.E. Logan, Biotechnol. Bioeng. 88 (2004) 854.

[20] F. Xiao, S.F. Yang, X.Y. Li, Sep. Purif. Technol. 63 (2008) 634.

[21] R.M. Wu, G.W. Tsou, D.J. Lee, Chem. Eng. J. 80 (2000) 37.

[22] T. Pietsch, R. Mehrwald, R. Grajetzki, J. Sens, T. Pakendorf, R. Ulrich, J. Kumpart, G. Matz, H. Markl, Water Res. 36 (2002) 2836.

[23] G.W. Tsou, R.M. Wu, P.S. Yen, D.J. Lee, X.F. Peng, J. Colloid Interface Sci. 250 (2002) 400.

[24] Z. Huang, D. Legendre, P. Guiraud, Chem. Eng. Sci. 68 (2011) 1.

[25] G.M. Quenot, J. Pakleza, T.A. Kowalewski, Exp. Fluids 25 (1998) 177.

[26] K. Reinhold-Lopez, A. Braeuer, A. Schmitt, N. Popovska-Leipertz, A. Leipertz, Chem. Eng. J. 184 (2012) 315.

[27] M. Raffel, C.E. Willert, J. Kompenhans, Particle Image Velocimetry: a Practical Guide, Springer: Berlin, 1998.

[28] F. Xiao, X.Y. Li, K.M. Lam, Water Sci. Technol.: Water Supply 7 (2007) 213.

[29] F. Xiao, K.M. Lam, X.Y. Li, R.S. Zhong, X.H. Zhang, Colloid Surf. A: Physicochem. Eng. Aspects 379 (2011) 27.

[30] R.S. Zhong, X.H. Zhang, F. Xiao, X.Y. Li, Z.H. Cai, Water Res. 45 (2011) 3981.

[31] W.P. He, J. Nan, H.Y. Li, S.N. Li, Water Res. 46 (2012) 509.

[32] J.J. Zhang, X.Y. Li, AIChE J. 49 (2003) 1870.

[33] X.Y. Li, Y. Yuan, H.W. Wang, Environ. Sci. Technol. 37 (2003) 292.

[34]   D.H. Li, J.J. Ganczarczyk, Water Res. 22 (1988) 789.

[35]   D.J. Lee, G.W. Chen, Y.C. Liao, C.C. Hsieh, Water Res. 30 (1996) 541.

[36]   D.H. Li, J.J. Ganczarczyk, Environ. Sci. Technol. 23 (1989) 1385.

[37]   B.E. Logan, A.L. Alldredge, Mar. Biol. 101 (1989) 443.

[38]   D.H. Li, J.J. Ganczarczyk, Water Res. 21 (1987) 257.

[39]   G.P. Sheng, H.Q. Yu, X.Y. Li, Biotechnol. Adv. 28 (2010) 882.